AADE-24-FTCE-028

A Nanoindentation Method to Evaluate Sealing and Plugging Agents Used in Water Based Drilling Fluids for Shale Formations

Nancy C. Zhou, CNPC USA; Yuanzhi Qu and Yuan Geng, CPET; Meng Lu and Janine Shipman, CNPC USA; Fuchen Liu and Songbing Yan, CPET; Guoping Zhang, University of Massachusetts Amherst

Abstract

To improve wellbore stability, sealing and plugging agent(s) (SPA) are typically added to drilling fluids when drilling shale formations with fractures. Systematic experimental work has been implemented to develop a nanoindentation method to evaluate SPA using drilled cuttings from the field.

X-ray diffraction (XRD) analysis was used to find the mineralogy of shale samples from the field interested. Representative samples were selected and prepared as shale assemblies for infiltration and nanoindentation tests. Several commercially available SPA were injected into shale samples using infiltration setup by flowing the SPA dispersion solutions through the shale assembly. Nanoindentation tests were then conducted under the continuous stiffness measurement mode to probe the mechanical properties of the untreated and SPA-treated shale samples. By comparing their mechanical properties, we evaluated the efficiency of several SPA to improve the Young's moduli *E* of shale samples.

Our experimental work introduced the latest advancements of nano instruments and pertient methods into drilling fluid research. A nanoindentation method is developed to evaluate SPA using easily accessible shale samples, e.g. cuttings. This method exhibits considerable potential as a valuable technique for drilling engineers.

Introduction

Nanoindentation is a nanoscale indentation technique to measure the mechanical properties of materials. These mechanical properties include elastic modulus, hardness, fracture toughness, creep parameters, and residual stress, to highlight a few. With the fast development of nano technologies, it is possible to precisely record the loading and unloading indentation process at a smaller scale, such as loading in nanonewtons (nN) and indentation depth in nanometers (Baker, 2001). Nanoindentation has been used to characterize the geomechanical behavior of small cutting samples obtained during drilling a well (Noya et al., 2023). The results from nanoindentation testing were compared with those from geotechnic modeling and from static and dynamic experiments of plug scales. These comparisons showed that the elastic modulus obtained by nanoindentation matches well the counterpart obtained by ultrasonic wave testing, and correlates to the ones obtained by macroscale triaxial compressive tests.

Thousands of wells are drilled each year worldwide in shale formations. The mechanical instability of shale still brings a lot of challenges to the drilling industry, especially for mid to deep shale formations. To improve wellbore stability during drilling, SPA with different particle sizes and chemistry are typically added to drilling fluids (Goud et al., 2006, Yan et al., 2015, Musa et al., 2022). There is no API recommended method to evaluate the efficiency of the plugging and sealing treatments for shale drilling. Many laboratory procedures for additive screening, such as the shale particle dispersion test, and other specialized devices for downhole condition evaluation, such as the pressure transmission test (van Oort, 1994), have been used over the years for evaluating drilling fluids regarding shale stability (Stowe et al., 2001, Akhtarmanesh et al., 2013, van Oort et al., 2016, Khramov et al., 2023). The basic screening tests are simple to execute but only provide limited information (Khramov et al., 2023). Conversely, the downhole condition evaluation devices are expensive. Moreover, most methods require a not easily accessible core plug to perform.

In this paper, nanoindentation tests were conducted under the continuous stiffness measurement (CSM) mode to probe mechanical properties. Specifically, the main focus is on Young's modulus ***E*** of shale samples before and after treated by SPA in this paper. By comparing the results of ***E*** from both untreated and SPA-treated samples, we evaluate several commercially available SPA additives and give recommendation to formulate them further in drilling fluid.

Materials and methodology

Materials

Shale samples (see Figure 1) were collected from well sites in two different fields. Samples A and B were from the field that used water-based drilling fluids for drilling. Samples C and D were from the field using oil-based drilling fluids.

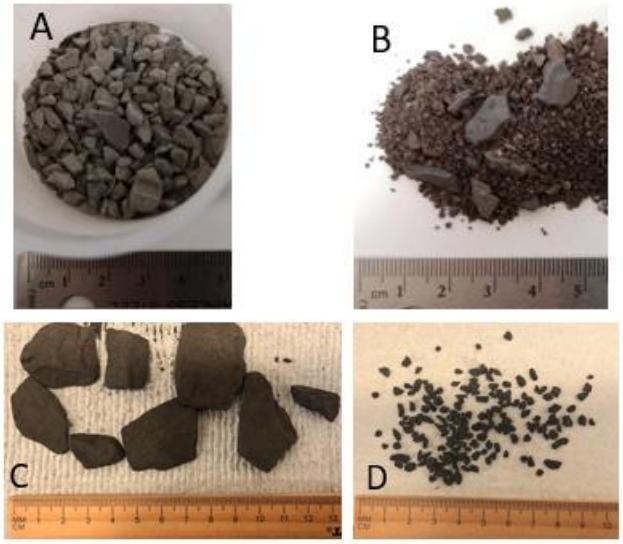

Figure 1 – Shale samples from field.

The SPA discussed in this paper are all commercially available products, see Table 1. Their mean particle sizes (PS) range from 20 nm to 7 µm, according to the particle size analyses performed using a Mastersizer 3000. Three liquid samples are dispersed in water media (SPA-1, SPA-2, and SPA-3, others two are solid powders (SPA-4 and SPA-5).

Table 1 The physical properties of SPA.

Sample #	Appearance	Water media	PS, D50, nm
SPA-1	Liquid	x	117
SPA-2	Liquid	x	20
SPA-3	Liquid	x	170
SPA-4	Solid		7090
SPA-5	Solid		200

Infiltration test

To simulate the drilling process, a modified flexible wall permeameter has been used to infiltrate SPA into shale samples, see Figure 2 (Zhou et al., 2020). During the infiltration test, SPA were dispersed into a liquid (e.g. water) to form a liquid suspension. The suspension was thoroughly homogenized via mixing and then dispered using an ultrasonic blender before the suspension was loaded into the double acting cylinder. It then was injected from the double acting cylinder through the manifolds to the small cap and filled the entire space of the top surface of the shale sample. The flow direction is shown in green arrows in Figure 2. Under a differential pressure of about 840 kPa, the SPA suspension went through shale samples. The exit flow was collected in the glass flask through the tube connected to the bottom cap of the sample assemblage system. The accumulated changes in the pump volume were recorded with time.

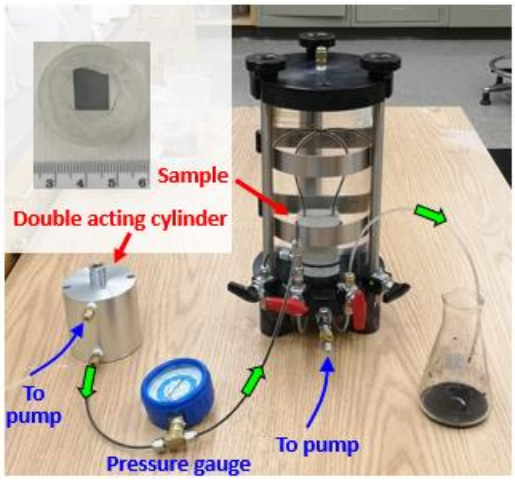

Figure 2 – Infiltration test set up (Zhou et al., 2020).

Nanoindentation test

Nanoindentation involves pushing a small and sharp indenter tip made of very hard materials, e.g., diamond, into a relatively softer sample, e.g., shales. Our nanoindentation tests were carried out in the Nano Indenter® G200 system equipped with a Berkovich diamond tip with a displacement resolution of < 0.01 nm and a load resolution of 50 nN. Indentation loading employed a CSM method, which imposed a small displacement-controlled harmonic oscillation with a frequency of 45 Hz and an amplitude of 2.0 nm on the primary monotonic loading signal and allowed the harmonic contact stiffness to be continuously determined. Hence, the Young's modulus $\boldsymbol{E}$ of the tested shale sample was determined as a function of indentation depth (h) (Oliver and Pharr, 1992). The accuracy of moduli measured by this method is within 5% comparing with values determined by other independent techniques such as elastic wave measurements.

The customized Berkovich diamond tip with a radius of less than 20 nm and an effective depth of greater than 25 µm was used for all tests. Load was applied at a constant indentation strain rate $\dot{h}/h$ of 0.05 s^{-1} to a preset maximum indentation depth (h_{max}) of 6000 nm, while the maximum achievable indentation depth was constrained by the instrument's load capacity of 620 mN. Because the harmonic contact stiffness was continuously determined, it led to a continuous extraction of depth-dependent data of Young's modulus $\boldsymbol{E}$, which was analyzed to track the property variations with depth. In addition, all indentation tests were run with an allowed thermal drift rate of less than 0.05 nm/s.

All indentation tests were run in a same loading direction to eliminate the possible influence of the shale anisotropy (Wu et al., 2020). Each specimen was conducted a total of 12 indent matrices, each of which consisted of a 10 X 10 grid with a spacing of 150 µm. They were conducted on different, randomly selected zones of the polished specimen surface. After the completion of each matrix of indents, four additional indents were made on fused silica. This silica is a standard calibration material to check and validate the tip condition. If the calibration results showed tip contamination or other

incorrect measurements, data from this prior matrix were discarded, and tip cleaning and recalibrating were conducted, and the test moved to the next matrix. This process was repeated 12 times to complete the measurements of 12 matrices.

Results and Discussions

Shale sample characterization.

Shale samples from the two fields were first characterized for their organic matter content, mineralogy by X-ray diffraction (XRD), and microfracture morphology. The organic matter content was estimated by the loss on ignition analysis. In this analysis, shale samples were first dried in the oven at 140°C and then ignited at 440°C. The loss of weight was recorded. For example, Sample A has an organic matter content of 1.67% (the average of 1.63% and 1.71%) and Sample C has an organic content of 7.67% (the average of 7.66%, 7.83% and 7.51%). In fact, Sample A is harder with a light gray color, while sample C is more fragmented and exhibits darker black color. The difference in the shales' coloration may be caused by their different organic matter contents.

Figure 3 – Loss on ignition analysis, sample C as an example.

Mineralogical compositions of these shale samples were analyzed by a Bruker D8 Advance X-ray diffractometer. The representative fragments of the shale samples were selected and wet ground with alcohol using a McCrone Micronizing Mill. The pulverized samples were then analyzed from 2 to 64 degrees two-theta (2θ) using a Cu *K*α radiation. JADE software was used to identify and quantify the mineralogy based on the Whole Pattern Fitting and Rietveld Refinement methods. Table 2 summarizes the whole rock mineralogy, with the clay minerals ranged from 28.6% to 56.1%. To match the mechanical property of individual phase from indentation results, the XRD results were grouped into four phases. For example, sample A is composed of quartz (29.5 wt.%), feldspar (total of 41.8%, including 32.9 wt.% plagioclase and 8.9 wt.% K-feldspar), clay minerals (with 12.3 wt.% illite, 4.0 wt.% chlorite, 4.9 wt.% kaolinite, and 7.4 wt.% muscovite), and others (including rutile, minor amorphous material, pyrite, calcite, etc.).

Table 2 Mineralogical and clay contents of shale samples characterized by XRD.

Sample	Quartz	Feldspar	Clay	Others
A	29.5	41.8	28.6	0.1
B	22	16	51	11
C	23.1	10.1	56.1	10.7
D	19	14	55	12

Microfracture characterization was performed through surface observations by scanning electron microscopy (SEM) and three-dimensional nondestructive imaging by X-ray computed tomography (XCT) to find the micro-fractures and/or pores in those shale samples. The XCT scanning results show that multiple cracks are irregularly distributed inside the sample with widths between 10 to 25 μm. Smaller fractures and pores with widths ranging from 50 to 250 nm are observed via SEM imagings. Microfractures are one of the dominant factors negatively affecting wellbore stability in many rock formations and fields (Abdallah et al., 2015). The selected SPA have been tested to seal and plug those microfractures by below infiltration and nanoindentation tests.

Infiltration

A total of 12 thin cuboidal specimens (~10 × 10 × 4 mm) were selectively trimmed from Sample A for the infiltration tests (IT). Before the injection, specimens were rehydrated by placing them in the desiccators above a synthetic pore fluid solution until no more weight changes were observed. The weight changes of the samples were measured periodically, and their water contents were correspondingly calculated. Figure 4 shows the rehydration curves for shale samples. All water contents increase significantly on the first day and gradually become stable after the sixth day. The final stable water content is in the range from 3.2 to 3.6 wt.% on the 17th day.

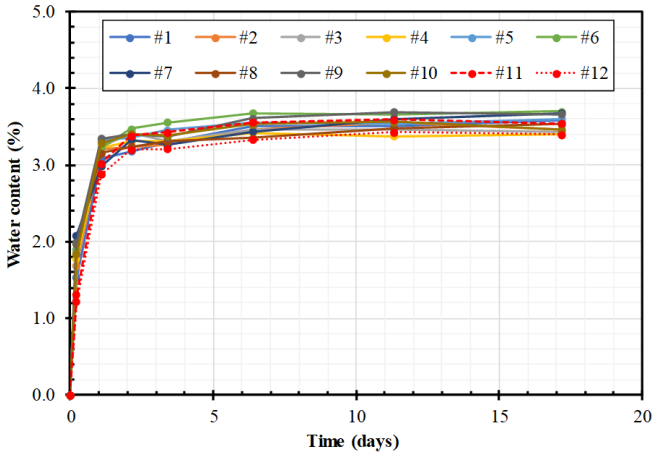

Figure 4 – Rehydration curves of specimens made from shale sample A.

Table 3 lists the infiltration tests of three specimens discussed in this paper. Infiltration tests of IT-1, IT-2 and IT-3 were designed to test the water-based SPA samples. IT-1 was a blank test with water, the dispersion solvent injected. The result of IT-1 was used as the baseline to compare the results of IT-2 and IT-3. We assumed that three specimens, S-I to S-III, all selected from rehydrated shale sample A in Figure 4 should have identical or similar permeability.

Table 3 Infiltration tests with different SPA solutions.

Infiltration test#	Specimens	SPA	Solution injected
IT-1	S-I	none	Water
IT-2	S-II	SPA-1	Water+SPA-1
IT-3	S-III	SPA-2	Water+SPA-2

Figure 5 shows infiltration results of IT-1 with the recording

of injected water volume versus time. The blue curve shows the time history of the pumped water volume, same as the injected solution volume with time, and the red curve is the temperature data log. This infiltration test took 23 days, with a final pump volume of about 1.3 mL. Because the infiltration curve fluctuates periodically with a negative correlation to the temperature log, we concluded that the fluctuation of the blue curve is caused by temperature changes during the test (Zhou et al. 2020). Due to the very low permeability of the shale, the temperature variation (or thermal change) alters the volumes of the tubes, pumps, cell, and the suspension, and this influence would be particularly significant for the volume measurements while testing super-low-permeability shales.

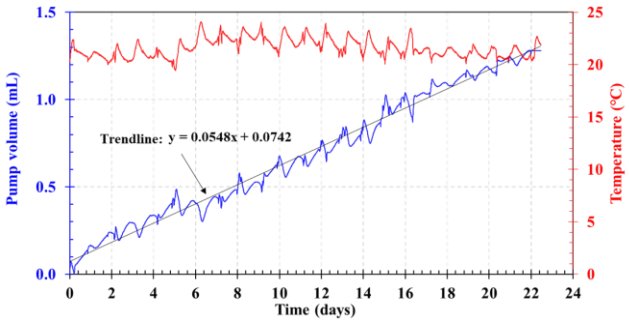

Figure 5 – Infiltration results of IT-1 for S-I.

The infiltration test was set up using a modified flexible wall permeameter. The original permeameter was designed to check the hydraulic conductivity, *K*c, using the slope of the pump volume verse time. In this test, the *K*c of water is estimated as 2.5E-13 m/s based on the slope of the trendline, shown in Figure 5. Therefore, the tested specimen (S-I) of shale sample A has a permeability of 25.9 nD, calculated using Darcy's equation. This permeability is the total permeability of S-I, and not the single permeability of the matrix or fractures. This permeability measurement matches well with those from the shale core samples recovered from the same field using pressure transmission tests (Zhou et al., 2020), 29.1 nD and 38.2 nD with artificial pore fluid (an low-salinity aqueous solution).

Figure 6 shows the infiltration curves of IT-2. It is not as linear as the curve of IT-1 in Figure 5 because of the SPA-1 injection. During the infiltration process of IT-2, the pump volume increased with a slope of 0.2225 mL/d for the first 2 days, which corresponds to an unplugged stage. Then the pump volume stayed the same for 0.75 days. This may indicate a plugged stage: SPA-1 temporarily blocked all the pores and flow channels. Because of the pressure difference (840 KPa) between the top and the bottom of S-II, the sealed SPA-1 was pushed away, or some induced fractures formed, more SPA-1 solution was pumped through from the 2.8 to 5 days. Then the pump volume stayed the same for another day, indicative of another plugging event. After another quick breakthrough of plugged stage with a sharp increase of pump volume, more solution could be injected with a slope of 0.1501 mL/d. Those observations demonstrate the efficiency of the SPA-1. It can plug the microfractures of S-II by holding the pressure up to 840 KPa for 1 day. It also slows down the beginning pump rate by 31.4% after the first "plug" was broken and then 32.5% (0.225 vs 0.1526, then vs 0.1501 ml/d).

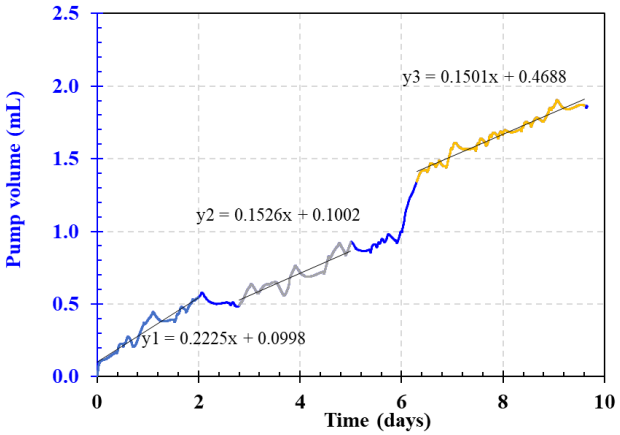

Figure 6 – Pump volume verse time of IT-2 for SPA-1.

Figure 7 shows infiltration curves of IT-3 for SPA-2. At the beginning of the infiltration process, the pump volumes increased with a slope of 0.0809 mL/d for the first 2.8 days. Then the pump volume stayed the same for 2.3 days. That indicates a plugged stage. After the sealed SPA-2 was pushed away, or some induced fractures appeared, more SPA-2 solution was pumped through with a slope of 0.046 mL/d. These observations demonstrate better efficiency of the SPA-2 than SPA-1. It can plug the microfractures of S-III, and hold the pressure up to 840 KPa for more than 2 days. After some plugs of SPA-2 was breakthrough, other remining plugs slowed down the beginning pump rate by 48.6%.

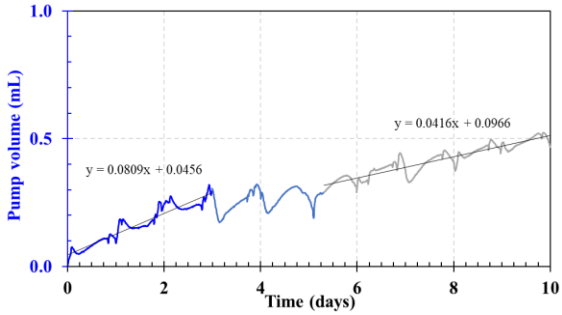

Figure 7 – Pump volume verse time of IT-3 for SPA-2.

Nanoindentation

Totally five specimens, S-I, S-II, S-III, and two additional S-01 and S-02 were characterized by big data nanoindentation technique as shown in Table 4. S-01 was prepared using shale sample A as it was received, not rehydrated. S-02 was a specimen rehydrated with a synthetic pore fluid solution.

Table 4 Summary of nanoindentation tests.

Nanoindentation test#	Specimens	*E*, GPa	Solution injected
NIT-1	S-01	29.2	none
NIT-2	S-02	27.9	none
NIT-3	S-I	25.4	Water
NIT-4	S-II	29.6	Water+SPA-1
NIT-5	S-III	30.86	Water+SPA-2

The data analysis process to obtain the average Young's modulus, ***E***, is shown in Figure 8 by using specimen S-01 as an example. First, the curves of load ***F*** verse indentation depth *h*, shown in Figure 8(a), were pre-screened. The corresponding residual indent images (e.g., indent geometry, coincidence of indentation points with pores or voids), referring to Figure 8(b), were carefully examined. The goal is to remove and discard any obvious outliers, ensuring that all data included in the statistical analysis are reliable. Then, the Young's modulus-depth (***E***-*h*) curves were graphed using the data calculated by the Oliver and Pharr method. To make the graph easy to read, only 49, not the total of 1200, indent results are shown in Figure 8(c). Then a cumulative distribution function-based deconvolution method was employed to extract the mechanical properties of individual phases. For a multiphase composite, the experimentally obtained Young's modulus of each phase is a random variate, assumed to follow the Gaussian distribution. Based on the XRD analysis, shown in Table 2, four mechanically different phases were determined from the data sets of nanoindentation results. The phases are respectively assigned as quartz, feldspar, clay matrix, and the interface between hard and soft phases. The deconvoluted results are shown in Figure 8(d).

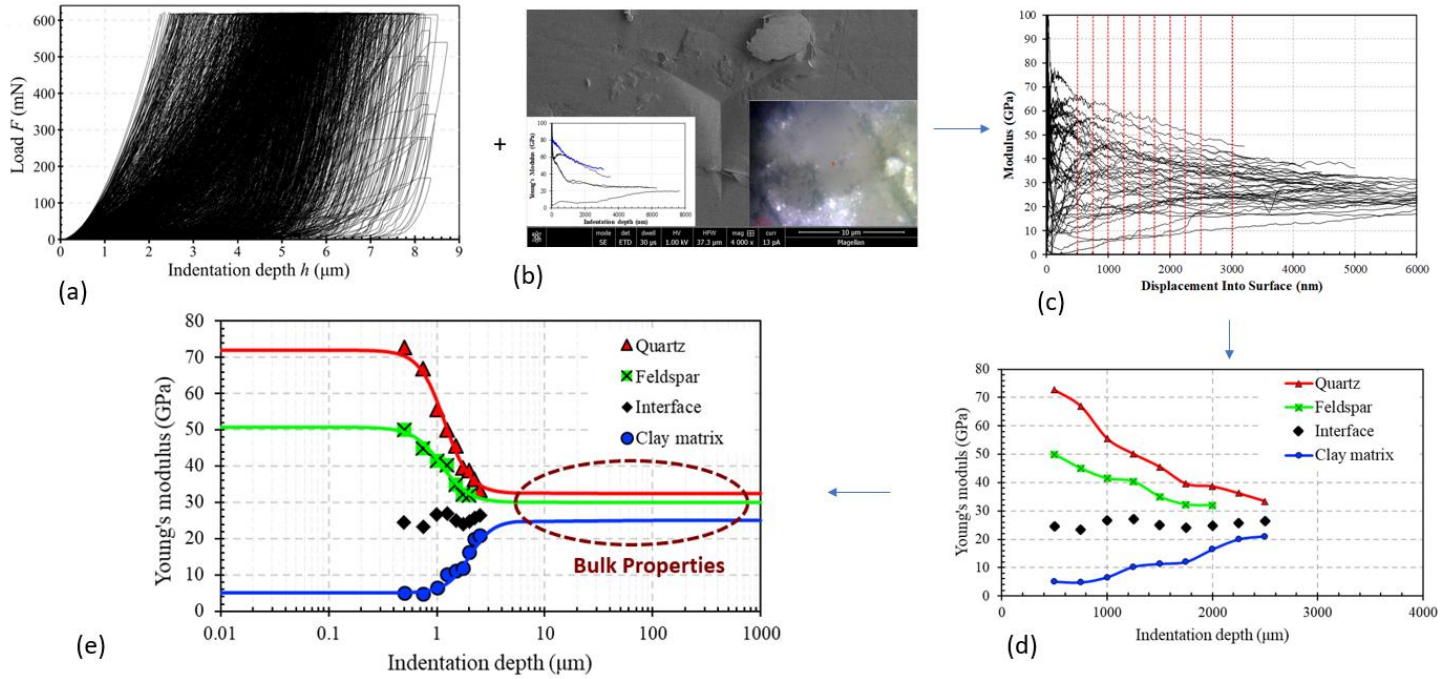

Figure 8 – Modulus results of NIT-1 for the base line.

In Figure 8(e), the indentation depth is plotted at a logarithmic scale to clearly show the trend at smaller depths and to ease the data-fitting of the indentation surround effect model. As shown in Figure 8(e), Young's modulus of relatively hard minerals gradually decreases with depth, while that of soft phases shows an increasing trend with depth. The fitting curves converge to a nearly constant value at larger depths. The average of these values at large depths is taken as the Young's modulus of the bulk rock, similar to the macroscopically measured ***E***. The average Young's modulus, expressing the bulk properties of shale specimen S-0, is 29.2 GPa, as listed in Table 4.

Using the above process, the other four Young's moduli ***E*** of the other four nanoindentation tests, NIT-2, NIT-3, NIT-4 and NIT-5, were obtained and listed in Table 4. Comparing results of NIT-2 with NIT-1, we concluded that the rehydration process is necessary. Without well-preserved shale samples from the field, Sample A received in the lab is not the same as the one in underground site. Rehydration resulted in about 3.4% weight gain. That led to a decrease on ***E*** by 4.5% (29.2 vs 27.9 GPa). Injection of water into S-I rehydrated specimen illustrated the mechanical property of ***E*** decreased more, from 27.9 GPa for S-02 to 25.4 GPa for S-I. Comparison of nanoindentation results from water injected specimen (S-I) versus that of SPA-1 injected specimen (S-II) showed that the Young's modulus, ***E***, increased by 16.5%, from 25.4 GPa of S-I to 29.6 GPa of S-II. Young's modulus, ***E***, of the specimen (S-III) after infiltration of SPA-2 was increased by 21.7%, from 25.4 GPa of S-I to 30.86 GPa of S-III. Those increases are significant enough to evaluate different kinds of SPA samples. The results are consistent with the infiltration results. Both results support that SPA-1 and SPA-2 are good candidates to seal and plug fractures/pores for our shale formation of interest. SPA-2 has better efficiency on lowering the hydraulic conductivity and increasing the Young's modulus, ***E***.

Conclusions and future work plan

In summary, a nanoindentation method was developed successfully to evaluate the SPA for wellbore stability using drilled cuttings from the field. This method includes the below steps.

1) Select and trim cuttings for the infiltration test.

2) Make specimens for microfracture characterization.

3) Run infiltration test with base fluid, for example, with water or salt solution for water-based drilling fluid.

4) Calculate the hydraulic conductivity, then estimate the permeability of the specimens.

5) Run infiltration test of the SPA and compare the results of the hydraulic conductivity at different stages and the time of the plugged stage to evaluate the sealing and plugging efficiency of the SPA.

6) Run nanoindentation tests of specimens, the one after infiltration test of base fluid, and the other one after infiltration test of SPA. Compare the average Young's modulus ***E*** of them to evaluate the improvement of mechanical property by the SPA.

In the next stage, SPA-4 and SPA-5 will be dispersed in water solution and evaluated by the above method. We also plan to evaluate some of the SPA listed in Table 1 for other shale samples shown in Figure 1.

Acknowledgments

The authors acknowledge the permission of CNPC USA to publish this paper. Special thanks to Yuchen Li, Yongkang Wu and Wei Sun of University of Massachusetts Amherst for their assistance on some experiments and data collection.

Nomenclature

SPA	*= Sealing and plugging agent(s)*
E	*= Young's moduli, GPa*
API	*= America petroleum institiute*
CSM	*= Continuous stiffness measurement*
PS	*=Particle size(s)*
D50	*= The mean or average particle size of a mineral*
nm	*= Nano meter*
µm	*= Micrometer*
nN	*= Nano Newtons*
nm/s	*= Nano meter per second*
mN	*= Mili-newtons*
XRD	*= X-ray diffraction*
XCT	*= X-ray computed tomography*
SEM	*= Scanning electron microscope*
IT	*= Infiltration test(s)*
Kc	*= Hydraulic conductivity, m/s*
S	*= Specimen(s)*
F	*= Load, mN*
h	*= Indentation depth, µm*
NIT	*= Nanoindentation test(s)*

References

1. Abdallah, K., El Sherbeny, W., Darwish, M., El Kammar, M., Gouda, M., Al Shaikh Nasser, S.A., Al-Hakim, M., 2015. "Formation Pressure Estimation & Miocene Clay Minerals Assemblages Identification, Drilling Challengers and Mitigation, Integrated Case Study, Gulf of Suez, Egypt." SPE Saudi Arabia Section Annual Technical Symposium and Exhibition, Al-Khobar, Saudi Arabia, 21-23 April, 2015. SPE-177981-MS. https://doi.org/10.2118/177981-MS
2. Akhtarmanesh S., Ameri Shahrabi, M. J., Atashnezhad, A. 2013. "Improvement of wellbore stability in shale using nanoparticles." Journal of Petroleum Science and Engineering,Volume 112, December 2013, Pages 290-295. https://doi.org/10.1016/j.petrol.2013.11.017
3. Baker, S.P. 2001. "Nanoindentation Techniques" in Encyclopedia of Materials: Science and Technology, pages 5908-5915. https://doi.org/10.1016/B0-08-043152-6/01030-5
4. Goud, M.C., Joseph, G. 2006. "Drilling Fluid Additives and Engineering to Improve Formation Integrity." SPE/IADC Indian Drilling Technology Conference and Exhibition, Mumbai, India, October 2006. SPE-104002-MS. https://doi.org/10.2118/104002-MS
5. Khramov, D., Panamarathupalayam, B., Barmatov, E. 2023. "Research, Evaluation of Laboratory Performance Tests for Drilling Fluids." AADE-23-FTCE-012. AADE Fluids Technical Conference and Exhibition, Midland, Texas, April 4-5, 2023. Available from https://www.aade.org
6. Musa, I., Hale, A., Mohandes, M. E. 2022. "Wellbore Strengthening – Continuous Application or Sweep as Needed?" AADE-22-FTCE-068, AADE Fluids Technical Conference and Exhibition, Houston, Texas, April 19-20, 2022. Available from https://www.aade.org
7. Noya, M., Celleri, H., Camilion E., Caneiro, A., Floridia, A., Grasetti, C.G., Ramallo, J.I., Fuertes, M.C. 2023. " Nanoindentation characterization of Vaca Muerta Formation shale rocks and its relation to geomechanical model and core plugs properties." ARMA 23-758, Rock Mechanics/Geomechanics Symposium, Atlanta, Georgia, 25-28 June 2023. https://doi.org/10.56952/ARMA-2023-0758
8. Oliver, W.C., Pharr, G.M.1992. "An improved technique for determining hardness and elastic modulus using load and displacement sensing indentation experiments." Journal of Materials Research 7, 1564–1583 (1992). https://doi.org/10.1557/JMR.1992.1564
9. Stowe, C., Halliday, W., Xiang, T., Clapper, D., Morton, K., Hartman, S. 2001. "Laboratory Pore Pressure Transmission Testing of Shale." AADE 01-NC-HO-44, AADE 2001 National Drilling Conference, "Drilling Technology- The Next 100 years", held at the Omni in Houston, Texas, March 27 - 29, 2001. Available from https://www.aade.org
10. van Oort, E. 1994. "A novel technique for the investigation of drilling fluid induced borehole instability in shales." SPEIISRM Rock Mechanics in Petroleum Engineering Conference held in Delft, The Netherlands, 29-31 August 1994. https://doi.org/10.2118/28064-MS
11. van Oort, E., Hoxha, B.B., Hale, A. 2016. " How to Test Fluids for Shale compatibility." AADE-16-FTCE-77, Available from https://www.aade.org
12. Wu, Y., Li, Y., Luo, S., Lu, M., Zhou, N., Wang, D., Zhang, G. 2020. "Multiscale elastic anisotropy of a shale characterized by cross-scale big data nanoindentation." International Journal of Rock Mechanics and Mining Sciences, Volume 134, October 2020, 104458, https://doi.org/10.1016/j.ijrmms.2020.104458
13. Yan, L., Li, C., Zhang, Z., Wang, J., Xu, X., Sun, J., Su, Y. 2015. "Successful Application of Unique High-Density Water-Based Drilling Fluid Used in Zhaotong Shale Gas Horizontal Wells." SPE/IATMI Asia Pacific Oil & Gas Conference and Exhibition, Nusa Dua, Bali, Indonesia, October 2015. SPE-176428-MS, https://doi.org/10.2118/176428-MS
14. Zhou, N., Wu, Y., Lu, M., Li, Y., Liu, F. Zhang, G. 2020. "An Experimental Study to Demonstrate That Nanoparticles Can Filter into Shale Formations and Improve Wellbore Stability." Abu Dhabi International Petroleum Exhibition & Conference,

Abu Dhabi, UAE, 9–12 November, 2020. SPE-202754-MS. https://doi.org/10.2118/202754-MS.